



Estimation of nocturnal ^{222}Rn soil fluxes over Russia from TROICA measurements

E. V. Berezina¹, N. F. Elansky¹, K. B. Moiseenko¹, I. B. Belikov¹, R. A. Shumsky¹, A. N. Safronov¹, and C. A. M Brenninkmeijer²

¹A.M. Obukhov Institute of Atmospheric Physics, Russian Academy of Sciences, Moscow, Russia

²Max-Planck-Institut für Chemie, Air Chemistry Division, Mainz, Germany

Correspondence to: E. V. Berezina (e_berezina_83@mail.ru)

Received: 13 May 2013 – Published in Atmos. Chem. Phys. Discuss.: 4 June 2013

Revised: 15 October 2013 – Accepted: 21 October 2013 – Published: 3 December 2013

Abstract. In TROICA (TRanscontinental Observations Into the Chemistry of the Atmosphere) campaigns (1999–2008), the simultaneous observations of near surface ^{222}Rn concentrations and atmospheric boundary layer thermal structure were performed along the Trans-Siberian Railway across northern Eurasia from Moscow to Vladivostok, including central, southern and far eastern parts of Russia. The data on ^{222}Rn and temperature vertical distribution are used to estimate ^{222}Rn regional scale soil fluxes based on calculations of nocturnal ^{222}Rn accumulation rates in the surface layer under inversion conditions. An effect of seasonal soil thawing on 2–4 times surface ^{222}Rn concentration increase from summer 1999 to autumn 2005 is observed. The estimated ^{222}Rn regional averaged fluxes vary over Russia from $29 \pm 8 \text{ mBq m}^{-2} \text{ s}^{-1}$ in its so-called European territory to $95 \pm 51 \text{ mBq m}^{-2} \text{ s}^{-1}$ in the southern area of Siberia. The highest ^{222}Rn fluxes are derived in the regions of high tectonic activity and orogenic belts of central and eastern Siberia and in far eastern Russia. The observed high ^{222}Rn flux variations in specific events show a strong effect of both soil and atmospheric conditions on ^{222}Rn near-surface abundance and the derived seasonal patterns over the continent.

1 Introduction

The radioactive gas radon (^{222}Rn) is one of the decay products of uranium-238 (^{238}U), the most abundant uranium isotope in the earth's crust. The main source of ^{222}Rn in the atmosphere is soil and its flux depends on the soil type and properties; its only sink is radioactive decay. ^{222}Rn is a chem-

ically inert gas with the half-life of 3.82 days. These features allow ^{222}Rn to be a useful tracer to study air transport (Prospero et al., 1970; Wilkniss et al., 1974, Dörr et al., 1983; Lee and Larsen, 1997) as well as to derive emissions of some atmospheric gases: CH_4 and CO_2 (Dörr et al., 1983; Gaudry et al., 1990; Levin et al., 1999; Moriizumi et al., 1996; Schmidt et al., 1996; Duenas et al., 1999; Biraud et al., 2000; Hirsch, 2007), N_2O (Biraud et al., 2000; Conen et al., 2002; Messenger et al., 2008; Corazza et al., 2011), CO (Messenger et al., 2008), and H_2 (Yver et al., 2009). ^{222}Rn is also commonly used for validating transport in climate models (Rasch, 2000; Szegvary et al., 2007), with ^{222}Rn flux being generally assumed to be spatially uniform with a rate of $1 \text{ atom cm}^{-2} \text{ s}^{-1}$ ($0.021 \text{ Bq m}^{-2} \text{ s}^{-1}$) from ice-free land surfaces and zero from oceans (Conen and Robertson, 2002). However, ^{222}Rn flux varies widely in space and in time. Therefore, the information about spatial and temporal ^{222}Rn flux variations over a variety of conditions is very important for correct estimation of spatial distribution and strength of natural and anthropogenic sources and sinks of greenhouse gases based on the observations of their near-surface concentrations.

^{222}Rn flux measurements were carried out in different regions of the world (Duenas et al., 1999; Turekian et al., 1977; Somashekarappa et al., 1996; Szegvary et al., 2007; Taguchi et al., 2011), including Russia (Milin et al., 1968; Kirichenko, 1970; Yakovleva, 2003; Tarasov, 2008). However, the data reported for Russia are not sufficient to form a clear picture of ^{222}Rn flux variations over such a vast territory.

During the last fifteen years the substantial data on ^{222}Rn spatial variability has been obtained with the use of a mobile carriage laboratory during international TROICA (TRanscontinental Observations Into the Chemistry of the Atmosphere) expeditions along the Trans-Siberian Railway from Moscow to Vladivostok (Elansky et al., 2009). These observations allow studying the large scale variability of near-surface atmospheric composition across extensive areas of the continent with essentially different geological, geographical and climatic features.

Preliminary results of ^{222}Rn flux estimation from TROICA expeditions are given in Berezina and Elansky (2009) (hereafter BE09). The method used in BE09 to calculate ^{222}Rn soil flux implies a uniform vertical ^{222}Rn distribution in a stable 100 m height surface layer based on the observations of ^{222}Rn vertical distribution in stable atmospheric conditions presented in some investigations (Jacobi and Andre, 1963; Servant, 1966 and Kataoka et al., 1998). Although such a simplification seems to be physically reasonable when studying particular events, it could lead to significant and poorly controlled errors in ^{222}Rn emission calculations when considering such a long-distance route with strongly variable conditions affecting ^{222}Rn fluxes.

In this paper we present a more elaborate procedure to assess regional-scale ^{222}Rn fluxes based on simultaneous observations of surface ^{222}Rn and temperature vertical distribution in the atmospheric boundary layer (ABL) during six TROICA expeditions in 1999–2008. The observational data along with the description of a simple numerical procedure to calculate vertical ^{222}Rn distribution within the nocturnal stable ABL are presented in Sect. 2. The observed regional-scale surface ^{222}Rn variability and derived ^{222}Rn fluxes are discussed in Sect. 3. Finally, the general conclusions on the results of this study are formulated in Sect. 4.

2 Data and methodology

The TROICA observational expeditions have been carried out on a regular basis since 1995 (Elansky et al., 2009) (Table 1). In this study we use the data from six expeditions in which the simultaneous measurements of ^{222}Rn and vertical temperature profiles in ABL were performed. The complete description of the measurement technique, data quality assessment and the data set obtained from the measurements from the railroad mobile laboratory are presented in Elansky et al. (2009).

The route of the TROICA expeditions overlaid on the radon risk map of Russia (Map of radon risk of Russia, 1996) (see discussion below in Sect. 3.1.1) is shown in Fig. 1. The total length of the route from Moscow to Vladivostok (9288 km) is covered for approximately 6 days, so the total duration of a single campaign (forward and return paths) is about two weeks. The strength of ^{222}Rn natural sources varies strongly along the route due to essentially different ge-

ological settings over the territory crossed by the railway. The significant part of the route is located in the mountain areas of the southern Urals and southern part of central and eastern Siberia where the ^{222}Rn surface fluxes are known to be elevated (see Fig. 1). As the railway runs along the most densely populated and industrial regions of the European part of Russia and southern area of Siberia, the anthropogenic origin of the measured ^{222}Rn concentrations (uranium deposits exploration and exploitation, mining and chemical combines, coal-fired power plants, nuclear power cycle factories) can also be important. We expect, however, that the relative effect of this signal is substantially diminished when inverting the radon flux values since the most of the data in each radon accumulation event is obtained either upwind of possible anthropogenic sources or in low wind synoptic conditions, so the characteristic time of advection from such sources is comparable with the ^{222}Rn lifetime.

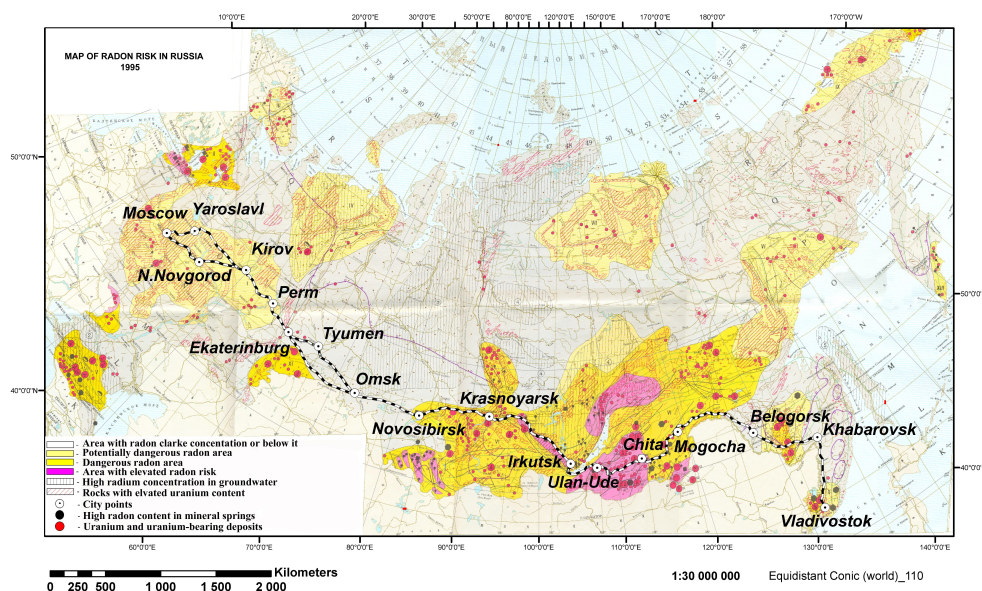
2.1 ^{222}Rn measurement technique

Surface ^{222}Rn concentration was measured by the analyzer of ^{222}Rn decay products LLRDM (Low Level Radon Daughters Measurement) produced by Tracer Lab (Germany). The air intake of the instrument is placed at the front side of the carriage roof at a 4 m height a.g.l. The measurements are founded in sampling of aerosol-attached radon daughters (^{218}Po , $t_{1/2} = 3.05$ min; ^{214}Pb , $t_{1/2} = 26.8$ min; ^{214}Bi , $t_{1/2} = 19.7$ min) through the quartz fiber filter ribbon of the instrument using air flow (150 L h^{-1}) driven by a pump. An integrated multi-channel analyzer of the LLRDM collects the alpha-spectrum of ^{222}Rn and its decay products in 256 channels. A microcomputer analyzes the spectrum and directly prints potential alpha energy concentration (PAEC) as well as activity concentration of single nuclides. PAEC describes the resulting α -energy of all decay products in a distinct volume until their total decay and common units are MeV L^{-1} or working level ($1\text{ WL} = 130\,000\text{ MeV L}^{-1}$). In the case of equilibrium between radon and its progenies, a stationary relation between radon gas concentration and the PAEC exists. The PAEC is often expressed as equivalent equilibrium concentration (EC or EEC). The EC value is in most cases lower than the real radon gas concentration in the air. The relation between EC and the radon gas concentration C_{Rn} is called equilibrium factor $F = \text{EC}/C_{\text{Rn}}$. The measured spectra as well as the calculated concentrations are saved in ASCII-files. The measurement range of the instrument is $0.1\text{--}100\text{ Bq m}^{-3}$. The result is available after 10 min and the instrument systematic errors are about 15 %.

The instrument uses a mathematical calibration method. Therefore, no radon chamber or comparison with other WL (working level) meters is necessary. There is no explicit mathematical formula available because an iterative method is used. The collection and the decay of the filter activity are simulated during the measurement. The microcomputer of the LLRDM integrates in real time the differential equations

Table 1. TROICA expeditions: dates and routes.

Expedition	Season	Time period	Route
TROICA-5	summer	26.06.99–02.07.99 03.07.99–13.07.99	N. Novgorod – Khabarovsk Khabarovsk – Moscow
TROICA-7	summer	27.06.01–03.07.01 04.07.01–10.07.01	Moscow – Khabarovsk Khabarovsk – Moscow
TROICA-8	spring	19.03.04–25.03.04 26.03.04–01.04.04	N. Novgorod – Khabarovsk Khabarovsk – Moscow
TROICA-9	autumn	04.10.05–10.10.05 11.10.05–18.10.05	Moscow – Vladivostok Vladivostok – Moscow
TROICA-11	summer	22.07.07–29.07.07 30.07.07–05.08.07	Moscow – Vladivostok Vladivostok – Moscow
TROICA-12	summer	21.07.08–28.07.08 29.07.08–04.08.08	Moscow – Vladivostok Vladivostok – Moscow

**Fig. 1.** Map of radon risk of Russia and the TROICA expeditions route along the Trans-Siberian Railway from Moscow to Vladivostok.

for 20 different initial sets of the radon daughters activity concentrations in the air: $C(\text{Po-218})$, $C(\text{Pb-214})$, $C(\text{Bi-214})$. Because of its short half-life, the concentration of Po-214 is in practice equal to the concentration of Bi-214. The result of the 20 simultaneous simulations are 20 pairs of calculated α -counts $N(\text{Po-218})$ and $N(\text{Po-214})$. The calculated α -counts of Po-218 and Po-214 for each of the 20 sets are compared with the real α -counts seen by the detector. The ratio of the air activities that fits best is taken to calculate the calibration factors for the potential α -energy and the radon daughters. The simulation calculates α -counts for a predefined fixed PAEC. The actual PAEC is calculated from both α -counts and the predefined PAEC. The activity of Po-218 and the concentration ratio Po-218 and Bi-214 are used to estimate the radon gas concentration:

$$C(\text{Rn}) = C(\text{Po} - 218) \cdot (C(\text{Po} - 218)/C(\text{Bi} - 214))^k,$$

where k is changed by using of new calibration factors.

The activity of the nuclides at the surface of the sampling filter increases during sampling. Therefore, the calibration factor of the instrument changes continuously too. In this paper the radon gas concentration data are analyzed.

2.2 Temperature profiles measurements

Vertical temperature profiles were measured with the use of the MTP-5 microwave temperature profiler (ATTEX, Russia) from the level of the carriage roof (4 m a.g.l.) up to the 600 m height (the in situ outdoor temperature measurements at 4 m a.g.l. were also conducted independently by standard meteorological thermometer). The MTP-5 measures the atmospheric thermal radiation in the center of the molecular-oxygen absorption band at around 56 GHz at different zenith

Table 2. Surface temperature inversion characteristics averaged in different seasons.

		Spring (TROICA-8)	Summer (TROICA-5,7,11,12)	Autumn (TROICA-9)
Inversion depth, m	average (\pm standard deviation)	220 \pm 145	210 \pm 119	198 \pm 101
	minimum	50	50	50
	maximum	500	600	600
Inversion intensity ($\Delta T = T_{\text{max}} - T_{4\text{m}}$), $^{\circ}\text{C}$	average (\pm standard deviation)	4.5 \pm 3.7	2.9 \pm 2.3	5.1 \pm 3.4
	minimum	0.2	0.2	0.2
	maximum	16.9	13.0	14.9
Inversion duration, min	average (\pm standard deviation)	300 \pm 210	245 \pm 170	365 \pm 300
	minimum	45	40	60
	maximum	860	710	990
Temperature gradient, $^{\circ}\text{C}/100\text{ m}$	average (\pm standard deviation)	1.9 \pm 0.9	1.3 \pm 0.6	2.5 \pm 1.3
	minimum	0.2	0.2	0.2
	maximum	6.6	10.7	8.9

angles. The brightness temperature is then retrieved from the measurements (Kadygrov and Pick, 1998) to obtain a vertical temperature profile in a range 0–600 m a.g.l. with 50 m vertical resolution. To minimize the effect of the electric locomotive and the short-term influence of different objects located near the railway on the instrument operation, zenith angle scanning was carried out at a 10° angle relative to the direction of the motion. The resolution of the retrieved temperature data is 5 min and the overall instrument accuracy is about 0.2°C . Some relevant parameters of the observed near-surface inversions (outside the large towns and their suburbs) are summarized in Tables 2 and 4.

2.3 Theoretical considerations

In the present study we use a simple numerical procedure to calculate ^{222}Rn accumulation rates in the stable nocturnal ABL for a number of specific accumulation events observed during the TROICA observations. For each event, we define t_1 the time of the beginning of surface inversion formation and t_2 the time of the observed maximum ^{222}Rn concentration, with the latter corresponding commonly to the time when the inversion starts to collapse. The time of a particular event varies from 3 to 13 h. Since the typical movement velocity of the mobile laboratory amounts to $50\text{--}70\text{ km h}^{-1}$, a characteristic spatial scale L for an individual event is within the range of 150–1000 km. Further, it seems to be appropriate to use the following major assumptions:

- i. during each event ^{222}Rn surface flux can be set to some constant value representing space and time averaged ^{222}Rn emission rate over L ;
- ii. at the time of inversion onset t_1 the surface ^{222}Rn concentration field is assumed to be spatially homogeneous over L ;
- iii. radon vertical transport due to diffusion is limited by the height of the inversion layer;
- iv. any changes in local ^{222}Rn concentrations in the near-surface layer below the inversion due to wind advection can be neglected compared to its vertical transport by eddy diffusivity.

The latter assumption is substantiated by the fact that during the observed strong surface temperature inversions horizontal air movement in ABL is generally very weak, so we do not consider air advection from any particular anthropogenic ^{222}Rn source and assume the main origin of ^{222}Rn under the inversion layer to be its soil flux. Hence, temporal evolution of ^{222}Rn vertical distribution under the inversion layer of the height H allows us to calculate the accumulation rate Q [Bq s^{-1}] for its total amount below H , which gives an estimate for ^{222}Rn soil flux as far as the assumptions (i to iv) hold. In this case, the general problem of atmospheric ^{222}Rn vertical and temporal variations reduces to the solution of a

non-stationary diffusion equation:

$$\frac{\partial c}{\partial t} = \frac{\partial}{\partial z} \left(K(z) \frac{\partial c}{\partial z} \right) - \lambda c, \quad z_0 < z < H(t), \quad t \in [t_1, t_2], \quad (1)$$

where c [Bq m^{-3}] is ^{222}Rn concentration, K [$\text{m}^2 \text{s}^{-1}$] is the height-dependent ^{222}Rn diffusivity, $\lambda (= 2.08 \times 10^{-6} \text{ s}^{-1})$ is the radon decay constant, and $z_0 (= 4 \text{ m a.g.l.})$ is the time independent measurement height at which $c_0 \equiv c(z_0, t \geq t_1)$ is the known function represented by the actually measured ^{222}Rn concentrations. The appropriate initial and boundary conditions for Eq. (1) are

$$c(z, t_1) = c_0(t_1), \quad (z_0 \leq z \leq H_{t=t_1}) \quad (2)$$

$$c(z_0, t) = c_0(t), \quad \left. \frac{\partial c}{\partial z} \right|_{z=H} = 0. \quad (t_1 < t < t_2) \quad (3)$$

Thus, according to Eq. (2) at the start time t_1 , ^{222}Rn concentration is equal to its value measured prior to the inversion formation and assumed to be uniformly distributed with height due to active daytime vertical mixing. A simple explicit time-forward second order space-centered scheme was used to solve Eqs. (1)–(3) on a 1-D grid with $\Delta_z = 1 \text{ m}$ grid spacing between adjacent vertical levels and with 6 s time step to satisfy general stability requirements for a chosen $K(z)$ profile. Once vertical distribution of radon is known, the total ^{222}Rn abundance M and accumulation rate Q within a layer $0 \leq z \leq H$ at a time t_i can be calculated:

$$M(t_i) = \int_0^H c(t, z) dz = \sum_j c(z_j, t_i) \cdot \Delta_z, \quad (4)$$

$$Q = \overline{\text{d}M/\text{d}t}^t \approx (M_{t=t_2} - M_{t=t_1}) / (t_2 - t_1), \quad (5)$$

where the summation is performed over the computational cells and a horizontal bar denotes time averaging.

In the case of strong inversion, the diffusion coefficient K near the earth's surface is known to be very weak, yet being quite variable with z depending on the vertical variations of wind velocity and stability. Following Cohen et al. (1972), we assume in the present study a linear dependence of K on z , with the upper-layer K being independent of height and in the surface layer below 100 m being given as

$$K(z) = K(z_1) \cdot z/z_1, \quad (z < H), \quad (6)$$

where $K(z_1)$ is some known diffusivity rate at a reference level. In our calculations the value of H is set to be constant and was chosen from numerical expeditions to be so high ($\sim 600 \text{ m}$) that it does not affect at any appreciable rate the final estimates of radon fluxes. We used the vertical diffusivity profiles from 1 m height above ground given

by Jacobi and Andre (1963) (their curves WNW and IWN in Fig. 1) used in the relevant studies on ^{222}Rn distribution (Beck and Gogolak, 1979; Moses et al., 1960). We derive a plausible range for warm-season $K(z_1)$ diffusivities along the TROICA route basing on the corresponding model values at heights 50–100 m a.g.l. from NOAA ARL Archived Meteorology database (<http://ready.arl.noaa.gov/READYamet.php>). We chose $K(z)$ profiles characteristic of two stability classes of ABL: $\Delta T_{100} > 4.0 \text{ }^\circ\text{C}$ – extremely stable (G), and $\Delta T_{100} = 1.5\text{--}4.0 \text{ }^\circ\text{C}$ – moderately stable (F), according to the common classification of Pasquill (1961) where ΔT_{100} is a temperature change in the near-surface 100 m layer. Table 2 shows the surface temperature inversion characteristics from the TROICA data set averaged for different seasons with the strongest positive temperature gradients observed in spring and autumn expeditions (TROICA-8 and 9), owing to anti-cyclonic weather conditions over the majority of the route. Hence, the selected classes G and F completely cover the range of ΔT_{100} values observed during the TROICA expeditions for nocturnal surface inversions. We apply

$$K(z_1) = \begin{cases} 10 \text{ cm}^2 \text{ s}^{-1} & \text{for class G,} \\ 100 \text{ cm}^2 \text{ s}^{-1} & \text{for class F.} \end{cases} \quad z_1 = 1 \text{ m}, \quad (7)$$

which are also in a good agreement with the results presented in Bezuglaya (1983) for Russian regions and with the average K values in a 90 m depth surface layer proposed in Hosler et al. (1983) for the F stability class. Since a particular value of the diffusivity rate has a first-order influence on the final estimates of ^{222}Rn fluxes, two series of the calculations with $K(z_1)$ value given by Eq. (7) were carried out to assess a plausible range of radon soil fluxes for each observational episode.

3 Results and discussion

3.1 Variations of surface ^{222}Rn concentration over Russia

3.1.1 ^{222}Rn spatial distribution

Figure 2 shows the spatial distribution of original 10 min mean ^{222}Rn concentrations and 10th, 50th and 90th percentiles calculated for 100 km parts of the route. For spring and autumn data only the 50th percentile values are considered because of a limited data set for calculations. The figure also presents the altitude a.s.l. along the Trans-Siberian Railway to demonstrate an importance of terrain elevation in the observed radon distribution. For the regional-scale representation, we divided the Russian territory along the Trans-Siberian Railway into 6 regions according to their basic geological features: ETR or European territory of Russia (Moscow-Perm), Ural (Perm-Ekaterinburg), western Siberia (Ekaterinburg-Novosibirsk), central Siberia (Novosibirsk-Irkutsk), eastern Siberia (Irkutsk-Belogorsk) and far eastern

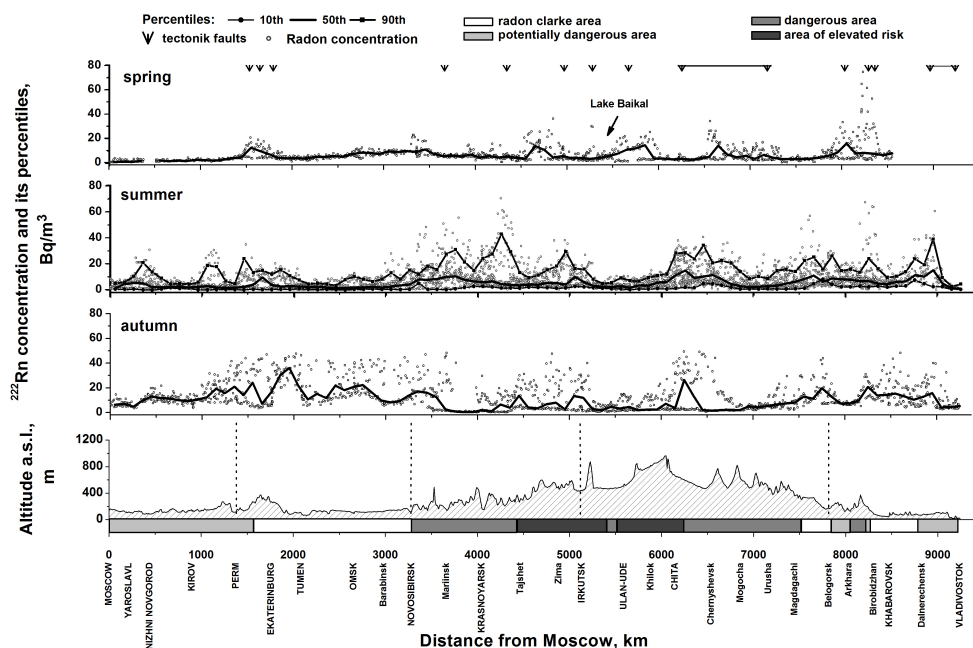


Fig. 2. Spatial distribution of surface ^{222}Rn concentration (10 min average values) and altitude a.s.l. from Moscow to Vladivostok in TROICA expeditions. The radon risk areas corresponding to the map of radon risk of Russia are presented as shaded rectangles. Percentiles are presented for 10 min radon values for each 100 km route part (for spring and autumn data only the 50th percentile values are presented because of a limited data set for calculations).

Russia (Belogorsk-Vladivostok). One can see from the figure that significant variations of radon concentrations exist in each season even within geologically uniform areas. It should be noted, however, that simple examination of the displayed time series does not provide any information about the true geographical areas of enhanced radon fluxes, since the measured surface concentrations depend strongly on vertical exchange rate driven by ABL daily variations and hence can be strongly connected to the local observation time. The marked increase in radon concentrations seen at some parts of the route is found to be controlled by a nighttime accumulation effect in temperature inversion conditions, which overrides the possible influence of other contributing factors. Some appropriate statistics on spatially averaged 1 h diurnal and daytime ^{222}Rn concentrations for each region and the inversion characteristics averaged for the Russian regions from the summer and autumn observations are shown in Tables 3 and 4, respectively. The spring inversion characteristics were not presented in Table 4 because of a lack of data for spatial averaging. The table shows that in most cases the diurnal mean ^{222}Rn concentrations are significantly higher for all seasons and regions than the daytime ones due to the nighttime accumulation effect (discussed in detail in Sect. 3.1.2.). However, seasonal ^{222}Rn concentrations spatially averaged for the different studied Russian regions (see Table 3) show high daytime mean radon concentrations in spring for the European territory and Ural region and in autumn for the European territory (ETR) and far eastern Russia region. Furthermore,

in the Eastern Siberia and far eastern Russia regions, spring ^{222}Rn concentrations are higher than the summer ones (about 2 times higher for far eastern Russia region). We suppose that prolonged temperature inversions existed up to midday hours in these observational periods in the regions under consideration (Tables 2 and 4) could contribute to such high daytime radon concentrations. The limited number of the expeditions performed in each season (see Table 1) does not allow us to completely filter out the nighttime accumulation signal from the observational data. We therefore describe here some large-scale features of spatial ^{222}Rn distribution based on daytime statistics (listed in Table 3) rather than on diurnal means, assuming the former to be more representative of background atmospheric radon levels over the continent. Nevertheless, spring daytime mean radon concentrations in the Ural and Western Siberia regions are also higher than summer ones. We suppose that it can be due to both snow melting in the regions mentioned during the TROICA campaigns, resulting in sharp radon increase in the air and the effect of regional ^{222}Rn sources. Both factors need to be investigated in detail in a special study.

According to Table 3, the highest daytime mean radon concentrations were observed in the far eastern Russia region (12.4 and 7.3 Bq m^{-3} in autumn and summer, respectively) and the central Siberia region (7.8 and 6.8 Bq m^{-3} in autumn and summer, respectively). According to the summer and spring expeditions, low daytime mean ^{222}Rn concentrations, $2\text{--}5 \text{ Bq m}^{-3}$, are typical for the ETR and Western Siberian

Table 3. Statistics on spatially averaged 1 h diurnal and daytime ²²²Rn concentrations for the studied Russian regions in different seasons (in Bq m⁻³). The numbers of the regions: I – Moscow-Perm (0–1380 km from Moscow); II – Perm-Ekaterinburg (1380–1904 km from Moscow); III – Ekaterinburg-Novosibirsk (1904–3283 km from Moscow); IV – Novosibirsk-Irkutsk (3283–5136 km from Moscow); V – Irkutsk-Belogorsk (5136–7818 km from Moscow); VI – Belogorsk-Vladivostok (7818–9242 km from Moscow).

No.	Region	Diurnal		Daytime			
		mean	st.dev	mean	st.dev	min	max
Spring							
I	European territory	2.0	0.9	2.0	1.2	0.4	3.9
II	Ural	4.9	2.7	5.0	3.9	2.6	14.3
III	Western Siberia	6.3	2.5	5.3	1.9	3.2	8.8
IV	Central Siberia	6.7	4.3	5.9	4.3	1.9	25.5
V	Eastern Siberia	8.0	6.5	4.4	3.8	0.3	16.9
VI	Far Eastern Russia	17.6	14.8	7.0	1.7	4.8	10.5
Summer							
I	European territory	4.0	4.5	2.1	3.5	0.1	21.0
II	Ural	6.9	7.1	4.7	1.1	0.5	4.1
III	Western Siberia	3.7	3.3	2.9	2.6	0.6	12.5
IV	Central Siberia	9.5	8.5	6.8	5.2	1.0	29.2
V	Eastern Siberia	7.5	6.6	4.6	4.1	0.3	33.4
VI	Far Eastern Russia	8.8	7.0	7.3	5.8	0.4	39.3
Autumn							
I	European territory	12.8	7.0	13.3	6.4	7.7	24.5
II	Ural	22.6	13.4	7.0	2.2	4.6	10.2
III	Western Siberia	22.3	10.9	17.9	10.6	6.9	38.2
IV	Central Siberia	11.3	10.2	7.8	6.5	0.6	18.4
V	Eastern Siberia	9.6	10.2	6.3	6.3	1.0	28.9
VI	Far Eastern Russia	12.4	7.2	12.4	7.0	6.7	28.4

Table 4. Surface temperature inversion characteristics averaged for the studied Russian regions from the summer and autumn expeditions. The numbers of the regions: I – Moscow-Perm (0–1380 km from Moscow); II – Perm-Ekaterinburg (1380–1904 km from Moscow); III – Ekaterinburg-Novosibirsk (1904–3283 km from Moscow); IV – Novosibirsk-Irkutsk (3283–5136 km from Moscow); V – Irkutsk-Belogorsk (5136–7818 km from Moscow); VI – Belogorsk-Vladivostok (7818–9242 km from Moscow).

No.	Region	Inversion depth, m			Inversion intensity ($\Delta T = T_{\max} - T_{4m}$), °C			Inversion duration, min		
		Average (\pm standard deviation)	minimum	maximum	Average (\pm standard deviation)	minimum	maximum	Average (\pm standard deviation)	minimum	maximum
Summer										
I	European territory	220 ± 120	50	600	2.7 ± 1.9	0.2	11.2	265 ± 150	71	500
II	Ural	150 ± 80	50	350	1.9 ± 1.3	0.2	5.6	160 ± 90	71	320
III	Western Siberia	200 ± 90	50	500	2.9 ± 1.9	0.2	9.4	275 ± 105	125	382
IV	Central Siberia	225 ± 130	50	600	3.3 ± 2.7	0.2	11.9	225 ± 170	55	608
V	Eastern Siberia	200 ± 130	50	600	2.7 ± 2.2	0.2	14.5	200 ± 170	40	672
VI	Far Eastern Russia	220 ± 115	50	600	3.1 ± 2.4	0.2	13.0	385 ± 215	105	711
Autumn										
I	European territory	128 ± 91	50	350	1.8 ± 1.5	0.2	6.7	291 ± 320	100	771
II	Ural	215 ± 89	50	350	4.8 ± 2.2	0.2	10.3	–	–	465
III	Western Siberia	265 ± 92	50	600	8.0 ± 3.1	0.2	14.9	435 ± 351	100	800
IV	Central Siberia	179 ± 91	50	350	4.7 ± 3.0	0.2	13.8	375 ± 382	105	645
V	Eastern Siberia	225 ± 114	50	600	5.7 ± 3.3	0.2	16.0	312 ± 331	60	991
VI	Far Eastern Russia	185 ± 82	50	350	4.1 ± 2.1	0.2	13.6	458 ± 341	70	861

Table 5. Seasonal variations of diurnal and daytime (no temperature inversions) mean ^{222}Rn concentrations along the Trans-Siberian Railway (in Bq m^{-3}).

		Average (\pm standard deviation)	Mode	Median	Maximum	Minimum	Lower quartile (25 %)	Upper quartile (75 %)
Summer	diurnal	7.2 ± 7.8	3.1	4.8	70.7	< 0.1	2.3	9.3
	daytime	4.5 ± 4.1	3.0	3.2	21.2	< 0.1	1.7	6.2
Autumn	diurnal	12.6 ± 10.9	5.2	9.3	49.4	0.2	4.2	17.5
	daytime	6.1 ± 4.7	2.2	5.1	29.6	0.2	2.2	8.9
Spring	diurnal	6.7 ± 6.7	3.6	4.7	74.8	0.2	3.0	7.8
	daytime	3.7 ± 2.1	3.6	3.3	13.4	0.3	2.3	4.6

regions characterized by flat terrain with low absolute elevations. However, in the autumn 2005 expedition, high daytime mean ^{222}Rn concentrations, up to 13 and 18 Bq m^{-3} in the ETR and Western Siberia, respectively, were observed (see Fig. 2 and Table 3). The probable reason of such radon increase is a cumulative effect of two factors: steady anticyclonic conditions with strong and prolonged (up to 16 h) surface temperature inversions and the existence of significant regional ^{222}Rn sources (mining operations, uranium deposits exposure and geological faults). On the whole, ^{222}Rn concentrations are higher in autumn compared to other seasons in the studied Russian regions (see Fig. 2 and Table 5). The factors which can determine such seasonal ^{222}Rn variations will be discussed further in Sects. 3.1.3 and 3.1.4.

Table 3 shows that there exists some negative correlation in near-surface radon abundances between the western (ETR to the western Siberia region) and eastern (central and eastern Siberia regions) parts of the continental areas of northern Eurasia. This feature was earlier observed in the seasonal variability of surface air abundances of other trace gases as well (Elansky et al., 2009) and can be most probably connected to a long-wave trough/ridge system that commonly persists over continental areas of northern Eurasia, including during the periods of the TROICA expeditions.

We compared ^{222}Rn concentrations from the TROICA expeditions with the map of radon risk of Russia (Maximovsky et al., 1996) compiled on the basis of the generalized analytical data on radiogeochimistry, radiometric investigation and other materials obtained from long-term research of different Russian scientific organizations. The authors of the map divided Russian territory into geographical areas according to the degree of radon risk, as shown in Fig. 2. According to the TROICA data, radon concentrations in the areas of elevated radon risk shown on the map are commonly lower than that measured in the dangerous areas (see Table 4 and Fig. 2). The observed high ^{222}Rn concentrations between Magdagachi and Arkhara (Fig. 2) cover both the radon dangerous area and the “radon Clarke” area (the area where ^{222}Rn concentration is equal or below its average in the earth’s crust) shown on the map of radon risk immediately to the west,

which is likely to be due to the prevailing effect of the local observation times as discussed above. Generally, ^{222}Rn concentrations measured in the TROICA expeditions (Fig. 2) are found to be in a good agreement with the earlier studies on the radon risk areas (Maximovsky et al., 1996) as well as spatial locations of tectonic faults, which confirms our general notion about the reliability of the obtained ^{222}Rn data set and its applicability to invert radon soil fluxes at a regional basis.

3.1.2 Effect of the atmospheric stability on surface ^{222}Rn concentration

In TROICA expeditions, the highest ^{222}Rn concentrations (up to 75 Bq m^{-3}) were commonly observed during the nights with strong and prolonged surface temperature inversions. Figure 3 shows the mean diurnal cycles of temperature inversion height and ^{222}Rn concentration in different seasons. The surface temperature inversions existed usually from 18:00–19:00 to 06:00–08:00 LT and from 17:00 to 09:00–10:00 LT in the warm and cold seasons, respectively (Fig. 3a). The highest radon concentrations, up to 30–35 Bq m^{-3} , were observed in the early morning (04:00–06:00 LT), being a result of nighttime accumulation below temperature inversion, prior to the beginning of inversion collapse and subsequent decrease in ^{222}Rn concentration as a factor of 3 to 5 on average owing to convective mixing. During the day there was an absence of significant temperature inversions (no nighttime near-surface radon accumulation episodes), meaning concentration did not change significantly during the day and for all seasons was 1.5–3.5 Bq m^{-3} (Fig. 3b with the caption “no inversions”).

Table 5 presents diurnal and daytime mean ^{222}Rn concentrations for the different seasons according to the TROICA measurements. The measurements performed under daytime inversion conditions were excluded from the present data to suppress the strong effect of the associated radon accumulation on the derived statistics, which resulted in daily mean ^{222}Rn concentrations being 1.5–2 times lower on average compared to the diurnal ones in all seasons. The highest diurnal and daytime mean ^{222}Rn concentrations were observed

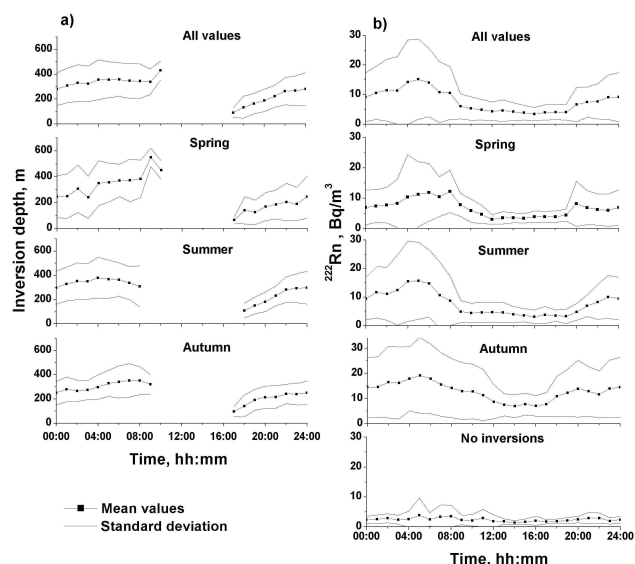


Fig. 3. The mean diurnal cycles of temperature inversion height (a) and ^{222}Rn concentration (b) from TROICA expeditions.

in autumn, owing to the strongest and most prolonged temperature inversions observed in this period (see Tables 2 and 4), which confirms significant influence of vertical exchange rates on surface ^{222}Rn variations at a seasonal scale.

3.1.3 Seasonal soil thawing effect on surface ^{222}Rn concentration

Along with vertical exchange due to the turbulent mixing, the soil (and its specific properties) is the other key factor affecting ^{222}Rn near-surface abundance. The soil covered with snow or ice accumulates ^{222}Rn , explaining its subsequent enhanced emission into the atmosphere during the first hours after snow melting (Miklyaev and Petrova, 2006). Commonly, the diffusion equilibrium between the soil and the surface atmospheric layer is reached in several hours, after which the radon flux attains its steady-state value; however, sometimes this process can last up to several days. Glover (2006) and Glover and Blouin (2007) note that the permafrost is a barrier to ^{222}Rn exhalation, resulting in its 80–90 % decrease in ambient air and 10–15 times increase in its abundance in the soil. Since the major part of the Trans-Siberian Railway in Eastern Siberia goes through the permafrost area, the influence of seasonal soil thawing should be accounted for when studying seasonal aspects of the ^{222}Rn surface flux variations. The thawing depth was calculated in the region 52–55° N, 105–130° E at the time periods of the TROICA campaigns using the scheme of the heat and moisture transfer in the soil (Arzhanov et al., 2008) in the ECHAM5/MPI-OM model (SRES A1B scenario). The resulting effect of the thawing depth on the near-surface radon abundance is shown in Fig. 4. The model-predicted thaw-

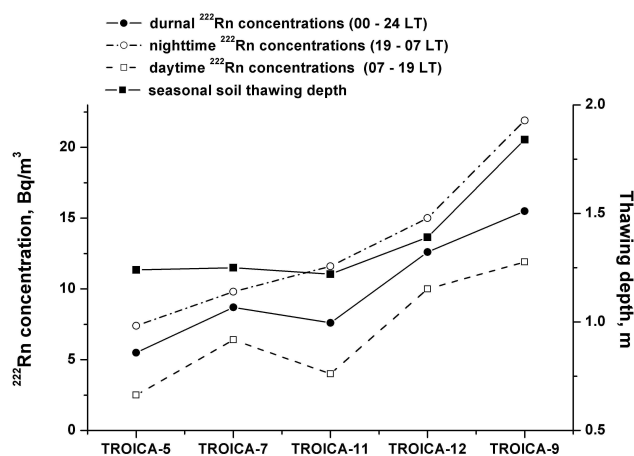


Fig. 4. Mean ^{222}Rn concentrations obtained from the TROICA data and the soil thawing depth calculated for the period of the expeditions in the region 52–55° N, 105–130° E using ECHAM5/MPI-OM model (SRES A1B scenario).

ing depth is approximately 1.24, 1.40 and 1.85 m for the summer TROICA-5,7,11, summer TROICA-12, and October TROICA-9 campaigns, respectively. One can see from the figure that near-surface radon concentrations increased more than 3 times (according to the daytime radon values) in this region from summer 1999 (TROICA-5) to summer 2008 (TROICA-12), reaching the highest value in autumn 2005 (TROICA-9), with the persistent increase in thawing depth being observed. To exclude the effect of the nighttime radon accumulation events, we divided nighttime and daytime data (see Fig. 4). Daytime mean ^{222}Rn concentrations (white squares in Fig. 4) are calculated for no temperature inversion conditions.

3.2 Nocturnal ^{222}Rn soil flux calculation

We use the measured ^{222}Rn concentrations in nocturnal accumulation events to estimate associated radon surface fluxes using the numerical approach discussed in Sect. 2.3. An example of ^{222}Rn flux calculation at the route part 1256–1076 km from Moscow 10 July 2001, 02:54–06:10 LT (TROICA-7), is presented in Fig. 6. The observed region is located in a flat area with a typical elevation from 150–200 m a.s.l. The figure shows the time series of the atmospheric temperatures at different heights a.g.l., the measured radon concentration, and the calculated total radon content varying approximately linear with time. Invoking Eq. (6), the regression slope of M on t gives the mean radon emission rate, which is an approximate estimate for Q .

In a particular nighttime accumulation event the atmospheric transport conditions within the surface inversion layer vary both with time and altitude. Hence, its resulting effect on radon accumulation rate can hardly be quantified at a rational basis, taking into account the lack of observational

Table 6. Weighted mean ^{222}Rn fluxes (calculated using the maximum-likelihood method) in Russian regions in different seasons. The numbers of the regions (km from Moscow): I – Moscow-Perm (0–1380 km); II – Perm-Ekaterinburg (1380–1904 km); III – Ekaterinburg-Novosibirsk (1904–3283 km); IV – Novosibirsk-Irkutsk (3283–5136 km); V – Irkutsk-Belogorsk (5136–7818 km); VI – Belogorsk-Vladivostok (7818–9242 km).

No.	Region	^{222}Rn flux (weighted mean error), $\text{mBq m}^{-2} \text{ s}^{-1}$	N (number of 10 min data points)
Spring			
I	European territory	–	–
II	Ural	52 (39)	26
III	Western Siberia	35 (28)	17
IV	Central Siberia	71 (50)	26
V	Eastern Siberia	59 (30)	28
VI	Far Eastern Russia	62 (43)	26
Summer			
I	European territory	29 (8)	101
II	Ural	50 (19)	19
III	Western Siberia	38 (12)	154
IV	Central Siberia	54 (13)	87
V	Eastern Siberia	63 (10)	193
VI	Far Eastern Russia	61 (15)	58
Autumn			
I	European territory	62 (31)	27
II	Ural	95 (51)	52
III	Western Siberia	95 (51)	22
IV	Central Siberia	39 (26)	80
V	Eastern Siberia	–	–
VI	Far Eastern Russia	65 (34)	85

data on the full set of parameters governing the turbulent mixing regime. In present simulations the major factor affecting the radon vertical distribution, and hence accumulation rate, is the vertical mixing rate profile controlled by the parameter $K(z_1)$. Since the exact value of the temperature gradient in a particular inversion event changes within a range of G and F stability classes, two sets of calculations were performed by setting $K(z_1)$ equal to 10 and $100 \text{ cm}^2 \text{ s}^{-1}$ according to Eq. (7) to obtain $Q(\text{G})$ and $Q(\text{F})$ values for radon accumulation rates for G and F stability classes, respectively. Accordingly, for each accumulation event i we define

$$\bar{Q}_i = (Q_G + Q_F)/2, \quad \sigma_{Q,i} = |Q_G - Q_F|/2 \quad (8)$$

as the best estimates for Q and an estimate error for \bar{Q}_i , respectively. The relative estimated error is commonly a few tens of percent and reaches as much as 50 % in some events. To make our estimates be representative at a regional scale, we calculate the expected means and associated errors as

$$\bar{Q}_{\text{reg}} = \sum_i g_i \cdot \bar{Q}_i / \sum_i g_i, \quad (9)$$

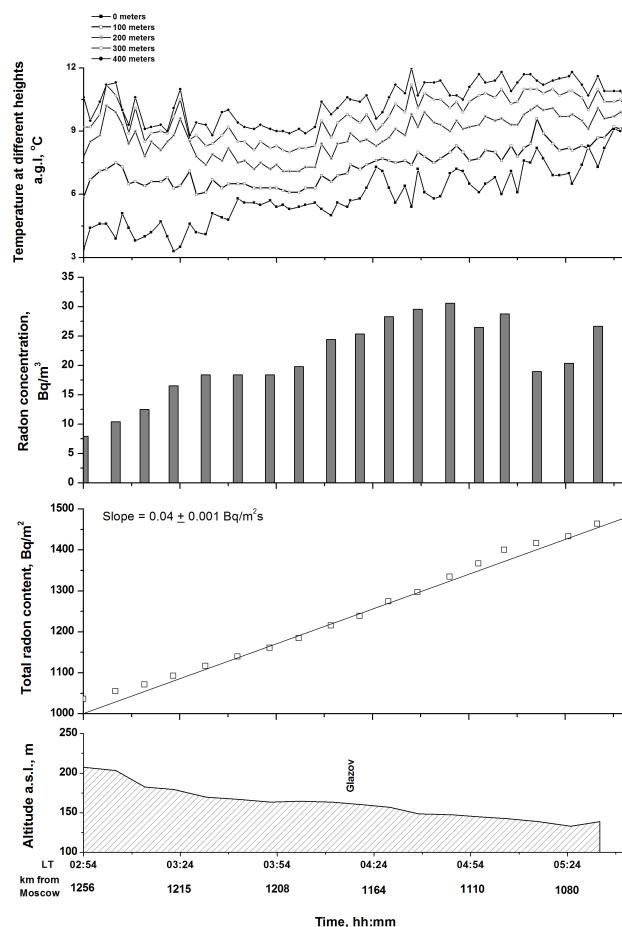


Fig. 5. Nocturnal ^{222}Rn flux calculation in stable atmospheric conditions at the route part 1256–1076 km from Vladivostok to Moscow (the East European region) 10 July 2001, 02:54–06:10 LT (the TROICA-7 expedition). Slope defines ^{222}Rn flux in this region. Glazov is the largest locality on the presented route.

and

$$\sigma_{Q,\text{reg}} = \left(\sum_i g_i \right)^{-2}, \quad (10)$$

respectively where $g_i = \sigma_{Q,i}^{-1}$, and summation by i is performed over all accumulation events observed during the TROICA expeditions within a particular region defined according to Fig. 2. The calculated weighted-mean region averaged radon soil fluxes are summarized in Fig. 6 and Table 6. One can see that the derived ^{222}Rn soil flux varies significantly over Russia, from $29 \pm 8 \text{ mBq m}^{-2} \text{ s}^{-1}$ to $95 \pm 51 \text{ mBq m}^{-2} \text{ s}^{-1}$, depending on the geological features as well as the seasons. The highest ^{222}Rn fluxes are derived in the mountain regions of central Siberia, eastern Siberia and far eastern Russia. In these Russian regions radon soil emissions are 1.5–3 times higher than in the plains (Table 6). In spring the weighted-mean region averaged ^{222}Rn

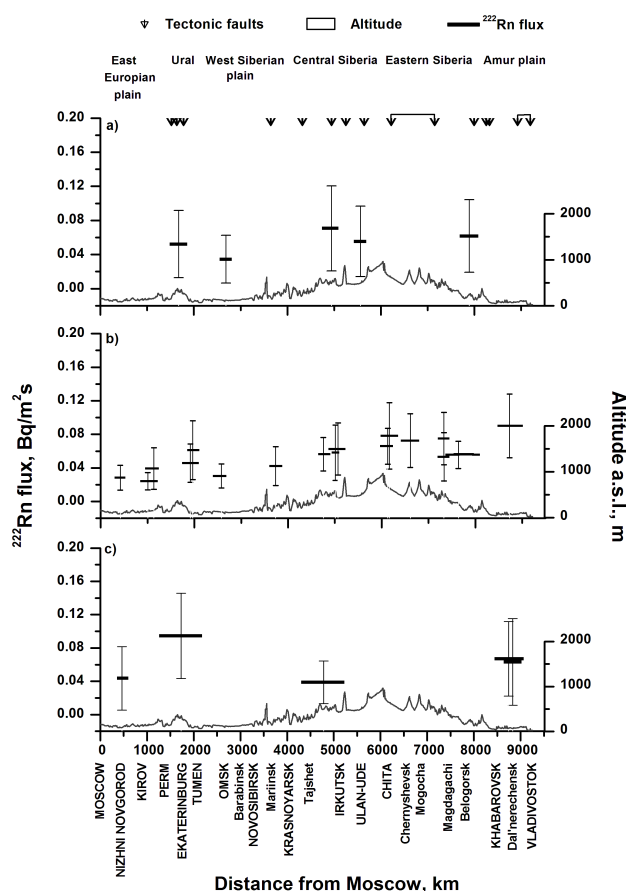


Fig. 6. ^{222}Rn soil fluxes over Russia calculated from the spring (a), summer (b) and autumn (c) expeditions. The length of each rectangle corresponds to the route part (in km) for which ^{222}Rn flux was estimated. The joined arrows indicate the strong faults crossing the route.

flux is higher and its variations are wider than in summer in the Ural, central Siberia and far eastern Russia regions.

Because of a wide range of turbulent mixing rates (conditions of which we will describe) chosen for ^{222}Rn flux estimation, we derived wide ^{222}Rn flux variations. We used two Kz profiles for calculations (see Eqs. 6 and 7) and derived two ^{222}Rn flux values (the boundary values in error bars). The mean ^{222}Rn flux is the average of two boundary values. The spatial variation is seen better in Fig. 6 from the mean ^{222}Rn fluxes than from its variations.

To observe an effect of the seasonal soil thawing on ^{222}Rn soil flux (see Sect. 3.1.3), we calculated the weighted mean ^{222}Rn flux for each expedition presented in Fig. 4. The estimated values do not show a significant increase from the summer expeditions to the autumn one. However, it is not correct to compare the mean ^{222}Rn fluxes calculated for each expedition because the ^{222}Rn flux episodes in the expeditions under consideration can differ geographically. So we chose the summer episodes (from all summer expeditions)

corresponding to the autumn episodes (in the same regions) and derived some increase in autumn weighted mean ^{222}Rn flux ($55.7 \pm 2.1 \text{ mBq m}^{-2} \text{ s}^{-1}$) compared to the summer one ($50.1 \pm 2.8 \text{ mBq m}^{-2} \text{ s}^{-1}$). The similar increase in both the seasonal soil thawing and ^{222}Rn concentrations is shown in Fig. 4. It can confirm the possible influence of the seasonal soil thawing on ^{222}Rn soil exhalation.

We compared ^{222}Rn fluxes calculated from the TROICA expeditions with the ^{222}Rn flux maps derived from the data modeling. Schery and Wasiolek (1998) proposed a global ^{222}Rn flux map based on a porous media transport theory and calibrated them with expedition ^{222}Rn flux data from Australia and Hawaii. The map gives ^{222}Rn flux for the Russian latitudes to be about $20\text{--}30 \text{ mBq m}^{-2} \text{ s}^{-1}$ but has a large uncertainty because of the lack of global data on soil moisture and ^{226}Ra content. Hirao et al. (2010) improved the performance of the model complimented by the soil and ^{226}Ra content and estimated the global ^{222}Rn flux density distribution for the period 1979–2007. These estimations give ^{222}Rn flux for Russian regions to be up to $30 \text{ mBq m}^{-2} \text{ s}^{-1}$. The ^{222}Rn flux estimations by Schery and Wasiolek (1998) and Hirao et al. (2010) are usually 4–5 times lower than the ones from TROICA measurements. The Russian ^{222}Rn flux map (<http://radon.unibas.ch>) generated by the scientific group from the University of Basel, Switzerland (Szegvary et al., 2007), and based on a gamma-dose rate map of Russia derived from aeroradiometric measurements (Map of natural gamma radiation doses of Russia, 1996) shows the highest radon fluxes in the studied regions of central and eastern Siberia; their estimations for far eastern Russia region correspond to ours. But according to the map, ^{222}Rn flux varies over Russia from 0.2 to $1.2 \text{ atom cm}^{-2} \text{ s}^{-1}$ (from 4 to $24 \text{ mBq m}^{-2} \text{ s}^{-1}$) which is 3–7 times lower than the range we inferred. It is possible that the wide range of the $K(z)$ values used for radon flux calculation could result in the overestimation of the mean radon flux values.

We also compared our results with the direct ^{222}Rn flux measurements reported for some Russian regions. According to the Perm CGMS radiation monitoring, in 2006 the mean ^{222}Rn flux was $40 \pm 10 \text{ mBq m}^{-2} \text{ s}^{-1}$ in Perm region (<http://wp.permecology.ru/report/report2006/17.html>) which corresponds to $40 \pm 20 \text{ mBq m}^{-2} \text{ s}^{-1}$ on average from the TROICA expeditions. ^{222}Rn soil fluxes in the city of Krasnoyarsk and its suburb Minusinsk are reported to vary from 14 to $20 \text{ mBq m}^{-2} \text{ s}^{-1}$ and from 9 to $60 \text{ mBq m}^{-2} \text{ s}^{-1}$, respectively (Voevodin and Kurguz, 2012; Sobyagina et al., 2012), being $40 \text{ mBq m}^{-2} \text{ s}^{-1}$ on average. These measurements are in a good agreement with our estimations for the Krasnoyarsk area ($40 \pm 30 \text{ mBq m}^{-2} \text{ s}^{-1}$). Kirichenko (1970) reported ^{222}Rn flux in the southern Ural region to be $11 \text{ mBq m}^{-2} \text{ s}^{-1}$ from the atmospheric radon profile studies in summer, which is lower than our estimations, $30\text{--}70 \text{ mBq m}^{-2} \text{ s}^{-1}$. The same author reported the mean ^{222}Rn flux in the European territory (Leningrad, Moscow, Kaluga city areas) in summer to be $7 \text{ mBq m}^{-2} \text{ s}^{-1}$. The mean ^{222}Rn

flux from the summer–autumn ^{222}Rn flux measurements in the Fyodorovskoe Forest Reserve, Tver region (the European part of Russia), presented in Levin et al. (2002) is $50\text{--}130\text{ mBq m}^{-2}\text{ s}^{-1}$. According to Milin et al. (1967), ^{222}Rn flux in Moscow region in summer is $38\text{ mBq m}^{-2}\text{ s}^{-1}$. Our estimations for the European territory of Russia (Moscow–Perm region) give the mean ^{222}Rn flux to be 29 ± 8 and $62 \pm 31\text{ mBq m}^{-2}\text{ s}^{-1}$ in summer and autumn, respectively.

Milin et al. (1967) reported the mean ^{222}Rn flux from summer measurements in Kirov to be $15\text{ mBq m}^{-2}\text{ s}^{-1}$, which is in agreement with our calculations ($20 \pm 10\text{ mBq m}^{-2}\text{ s}^{-1}$). Miklyaev and Petrova (2006) measured ^{222}Rn flux at different sites in Moscow and reported that ^{222}Rn flux varies from 5 to $72\text{ mBq m}^{-2}\text{ s}^{-1}$ ($21 \pm 12\text{ mBq m}^{-2}\text{ s}^{-1}$ on average) and from 4 to $264\text{ mBq m}^{-2}\text{ s}^{-1}$ ($38.6 \pm 34.4\text{ mBq m}^{-2}\text{ s}^{-1}$ on average) in the regions with sandy and clay soils, respectively. ^{222}Rn fluxes calculated from the observations on the mobile laboratory around Moscow (TROICA-10, 4–7 October 2006) at two observational parts of the Moscow region: (1) from Zhilino to Voskresensk, where sandy soils are spread, are $13 \pm 12\text{ mBq m}^{-2}\text{ s}^{-1}$; (2) from Jaganovo – Orekhovo-Zuyevo – Dmitrov, where both clay and sandy soils are spread, are $27 \pm 20\text{ mBq m}^{-2}\text{ s}^{-1}$.

4 Conclusions

The most significant variations in surface radon concentrations along the Trans-Siberian Railway are caused by the diurnal change in the ABL stability. The highest ^{222}Rn concentrations (up to 75 Bq m^{-3}) were usually observed during nighttime strong and prolonged temperature inversions in the mountain regions of Russia (central and eastern Siberia and far eastern Russia regions). Due to weak vertical mixing in the stable atmosphere, ^{222}Rn accumulates in ASL and its concentrations increased several times compared to its values during unstable atmospheric conditions. If we know the rate of ^{222}Rn accumulation in the nighttime stable ABL and the height of its mixing layer, we can estimate nocturnal radon soil flux.

The nocturnal ^{222}Rn soil flux calculated from the simultaneous measurements of ^{222}Rn and vertical temperature profiles in ABL in six expeditions from Moscow to Vladivostok varies over continental Russia from $29 \pm 8\text{ mBq m}^{-2}\text{ s}^{-1}$ to $95 \pm 51\text{ mBq m}^{-2}\text{ s}^{-1}$, depending on the geological features as well as the seasons. The highest ^{222}Rn soil flux values are derived for the mountain regions of central and eastern Siberia and far eastern Russia. Generally, ^{222}Rn concentration and flux over Russia peak in autumn and bottom out in spring. We suppose that there is a contribution of seasonal soil thawing to high radon concentrations and fluxes in the permafrost regions in autumn. However, there are some episodes with high ^{222}Rn concentrations (Ural and eastern Siberia regions) and fluxes (Ural, central Siberia and far eastern Russia regions) in spring. We suppose that possible snow

melting in these regions during the spring TROICA campaigns or/and air advection from local and regional radon sources could result in sharp radon increase in the air. Further detailed investigations are required.

It is possible that the wide range of the $K(z)$ values used for radon flux calculation could result in the overestimation of the mean radon flux values. As a whole, ^{222}Rn fluxes estimated from the expeditions on the mobile laboratory are in agreement with the direct measurements reported for Russian regions in literature.

The results presented in this paper can be important to investigate and document in detail the trends in fluxes of N_2O , CO_2 , and CH_4 during the coming decades of global warming in the late Holocene or so-called mid-Anthropocene.

Acknowledgements. The authors thank P. Crutzen, H. Paretzke, G. S. Golitsin, O. V. Lavrova, A. I. Skorokhod for their support, active participation in the organization and/or carrying out of the TROICA expeditions; I. B. Belikov and R. A. Shumsky for providing the expedition data; M. M. Arzhanov for the calculation of the seasonal thawing depth under permafrost conditions in the periods of the TROICA expeditions; and A. N. Safronov for his help with ArcView GIS data processing. The work is supported by the Russian Basic Research Foundation (projects no. 13-05-00461, 10-05-00272) and the 4th RAS Presidium Program.

Edited by: C. Gerbig

References

- Arzhanov, M. M., Eliseev, A. V., Demchenko, P. F., Mokhov, I. I., and Khon, V. Ch.: Simulation of thermal and hydrological regimes of Siberian river watersheds under permafrost conditions from reanalysis data, *Izvestiya, Atmos. Ocean. Phys.*, 44, 83–89, 2008.
- Beck, H. and Gogolak, C.: Time-dependent calculations of the vertical distribution of ^{222}Rn and its decay products in the atmosphere, *J. Geophys. Res.*, 84, 9C0385, 3139–3148, 1979.
- Berezina, E. V. and Elansky, N. F.: ^{222}Rn concentrations in the atmospheric surface layer over continental Russia from observations in TROICA expeditions, *Izvestiya, Atmos. Ocean. Phys.*, 45, 757–769, 2009.
- Bezuglaja, E. Yu.: *Climate Characteristics of Species Spreading Conditions in the Atmosphere*, Gidrometeoizdat, Leningrad, 326 pp., 1983.
- Biraud, S., Ciais, P., Ramonet, M., Simmonds, P., Kazan, V., Monfray, P., O'Doherty, S., Spain, T., and Jennings, S.: European greenhouse gas emissions estimated from continuous atmospheric measurements and radon-222 at Mace Head., *J. Geophys. Res.*, 105, 1351–1366, 2000.
- Cohen, L. D., Barr, S., Krablin, R., and Newstein, H.: Steady-state vertical turbulent diffusion of radon, *J. Geophys. Res.*, 77, 2654–2668, 1972.
- Conen, F. and Robertson, L. B.: Latitudinal distribution of Rn-222 flux from continents, *Tellus*, 54B, 127–133, 2002.
- Corazza, M., Bergamaschi, P., Vermeulen, A. T., Aalto, T., Haszpra, L., Meinhardt, F., O'Doherty, S., Thompson, R., Moncrieff, J.,

- Popa, E., Steinbacher, M., Jordan, A., Dlugokencky, E., Brühl, C., Krol, M., and Dentener, F.: Inverse modelling of European N₂O emissions: assimilating observations from different networks, *Atmos. Chem. Phys.*, 11, 2381–2398, doi:10.5194/acp-11-2381-2011, 2011.
- Dörr, H., Kromer, B., Levin, I., Münnich, K., and Volpp, H.: CO₂ and radon as tracers for atmospheric transport, *J. Geophys. Res.*, 88, 1309–1313, 1983.
- Druilhet, A., Guedalia, D., Fontan, J., and Laurant, J.: Study of radon 220 emanation deduced from measurement of vertical profiles in the atmosphere, *J. Geophys. Res.*, 77, 6508–6514, 1972.
- Dueñas, C., Fernandez, M. C., Cañete, S., Carretero, J., and Liger, E.: ²²²Rn concentrations, natural flow rate and the radiation exposure level in the Nerja Cave, *Atmos. Environ.*, 33, 501–510, 1999.
- Elansky, N. F., Belikov, I. B., Berezina, E. V., Brenninkmeijer, C. A. M., Buklikova, N. N., Crutzen, P. J., Elansky, S. N., Elkins, J. V., Elokhov, A. S., Golitsyn, G. S., Gorchakov, G. I., Granberg, I. G., Grisenko, A. M., Holzinger, R., Hurst, D. F., Igaev, A. I., Kozlova, A. A., Kopeikin, V. M., Kuokka, S., Lavrova, O. V., Lisitsyna, L. V., Moeseenko, K. B., Oberlander, E. A., Obvintsev, Yu. I., Obvintseva, L. A., Pankratova, N. V., Postilyakov, O. V., Putz, E., Romashkin, P. A., Safronov, A. N., Shenfeld, K. P., Skorokhod, A. I., Shumsky, R. A., Tarasova, O. A., Turnbull, J. C., Vartiainen, E., Weissflog, L., and Zhernikov, K. V.: Atmospheric Composition Observations over Northern Eurasia using the Mobile Laboratory: TROICA expedition, edited by: Elansky, N. F., Agrosplas, Moscow, Russia, 72 pp., 2009.
- Gaudry, A., Polian, G., Ardouin, B., and Lambert, G.: Radon-calibrated emissions of CO₂ from South Africa, *Tellus B*, 42, 9–19, 1990.
- Glover, P. W. J.: Increased domestic radon exposure caused by permafrost thawing due to global climate change, EGU General Assembly, Vienna, Austria, 2–7 April, EGU06-A-01439, 2006.
- Glover, P. W. J. and Blouin, M.: Modelling increased soil radon emanation caused by instantaneous and gradual permafrost thawing due to global climate warming, EGU General Assembly, Vienna, Austria, 15–20 April, EGU2007-A-07657, 2007.
- Hirao, S., Yamazawa, H., and Moriizumi, J.: Estimation of the Global ²²²Rn Flux Density from the Earth's Surface, *Jpn. J. Health Phys.*, 45, 161–171, 2010.
- Hirsch, A. I.: On using radon-222 and CO₂ to calculate regional-scale CO₂ fluxes, *Atmos. Chem. Phys.*, 7, 3737–3747, doi:10.5194/acp-7-3737-2007, 2007.
- Hosler, C. R.: Meteorological Effects on Atmospheric Concentrations of Radon (Rn-222), RaB (Pb-214), and RaC (Bi-214) Near the Ground, *Mon. Weather Rev.*, 94, 89–99, 1966.
- Jacobi, W. and Andre, K.: The vertical distribution of radon-222, radon-220 and their decay products in the atmosphere, *J. Geophys. Res.*, 68, 3799–3814, 1963.
- Kadyrov, E. N. and Pick, D. R.: The potential for temperature retrieval from an angular scanning single-channel microwave radiometer and some comparison with in situ observations, *Meteorol. Appl.*, 5, 393–404, 1998.
- Kataoka, T., Yunoki, E., Shimizu, M., Mori, T., Tsukamoto, O., Ohashi, Y., Sahashi, K., Maitani, T., Miyashita, K., Fujikawa, Y., and Kudo, A.: Diurnal Variation in Radon Concentration and Mixing-Layer Depths, *Bound.-Lay. Meteorol.*, 89, 225–250, 1998.
- Kirichenko, L. V.: Radon Exhalation from Vast Areas According to Vertical Distribution of its Short-Lived Decay Products, *J. Geophys. Res.*, 75, 3639–3649, 1970.
- Lee, H. N. and Larsen, R. J.: Vertical Diffusion in the Lower Atmosphere Using Aircraft Measurements of Radon-222, *J. Appl. Meteor.*, 36, 1262–1270, 1997.
- Levin, I., Glatzer-Mattheier, H., Marik, T., Cuntz, M., Schmidt, M., and Worthy, D. E.: Verification of German methane emission inventories and their recent changes based on atmospheric observations, *J. Geophys. Res.*, 104, 3447–3456, 1999.
- Levin, I., Born, M., Cuntz, M., Langendörfer, U., Mantsch, S., Naegler, T., Schmidt, M., Varlagin, A., Verclas, S., and Wagenbach, D.: Observations of atmospheric variability and soil exhalation rate of radon-222 at a Russian forest site. Technical approach and deployment for boundary layer studies, *Tellus B*, 54, 462–475, 2002.
- Map of natural gamma radiation doses of Russia: 1:10 000 000 scale, Explanatory notes, edited by: Vysokostrovskaya, E. B., Danilov, V. S., Krasnov, A. I., and Reshetov, V. V., M.-SPb.: Roscomnedra, 1996.
- Map of radon risk of Russia: 1:10 000 000 scale, Explanatory notes, edited by: Maximovsky, V. A., Smyslov, A. A., Kharlamov M. G., M.-SPb., 1996 (Roscomnedra, VSEGEI, Goscomvus, SP-bGGI).
- Messenger, C., Schmidt, M., Ramonet, M., Bousquet, P., Simmonds, P., Manning, A., Kazan, V., Spain, G., Jennings, S. G., and Ciais, P.: Ten years of CO₂, CH₄, CO and N₂O fluxes over Western Europe inferred from atmospheric measurements at Mace Head, Ireland, *Atmos. Chem. Phys. Discuss.*, 8, 1191–1237, doi:10.5194/acpd-8-1191-2008, 2008.
- Miklyaev, P. S. and Petrova, T. B.: Radon hazard in Moscow, Russia, IAEG2006 Engineering geology for tomorrow's cities, Pre-Congress Proceeding, The 10th IAEG International Congress, Nottingham, UK, 355–361, 2006.
- Milin, V. B., Malakhov, S. G., Zorina, K. I., and Sisigina, T. I.: Radon concentration and vertical turbulent mixing in the lowest atmospheric layer, Foreign technology div Wright-Patterson AFB, Ohio, 9 February, AD0679719, 1968.
- Moriizumi, J., Nagamine, K., Iida, T., and Ikebe, Y.: Estimation of areal flux of atmospheric Methane in an urban area of Nagoya, Japan, Inferred from atmospheric radon-222 data Atmospheric Environment Vol. 30, Nos 10/11, 1543–1549, 1996.
- Moses, H., Stehney, A. F., and Lucas, H. F.: The effect of meteorological variables upon the vertical and temporal distribution of atmospheric radon, *J. Geophys. Res.*, 66, 1223–1238, 1960.
- Pasquill, F.: The Estimation of the dispersion of windborne material, *Meteorological Magazine*, 90, 33–49, 1961.
- Prospero, J. M., Bonatti, E., Schubert, E., and Carlson, T. N.: Dust in the Caribbean atmosphere traced to an African dust storm, *Earth Planet. Sci. Lett.*, 9, 287–293, 1970.
- Rasch, P. J., Feichter, J., Law, K., Mahowald, N., Penner, J., Benkovitz, C., Genthon, C., Giannakopoulos, C., Kasibhatla, P., Koch, D., Levy, H., Maki, T., Prather, M., Roberts, D. L., Roelofs, G. J., Son, S. D., Stockwell, Z., Taguchi, S., Kritz, M., Chipperfield, M., Baldocchi, D., McMurry, P., Barrie, L., Balkanski, Y., Chatfield, R., Kjellstrom, E., Lawrence, M., Lee, H. N., Lelieveld, J., Noone, K. J., Seinfeld, J., Stenchikov, G., Schwartz, S., Walcek, C., and Williamson, D.: A comparison of scavenging and deposition processes in global models: results from the

- WCRP Cambridge Workshop of 1995, *Tellus*, 52B, 1025–1056, 2000.
- Schery, S. D. and Wasiolek, M. A.: Modeling radon flux from the earth's surface, *Radon and Thoron in the Human Environment*, edited by: Katase, A. and Shimo, S., 207–217, World Scientific, Singapore, 1998.
- Schmidt, M., Graul, R., Sartorius, H., and Levin, I.: Carbon dioxide and methane in continental Europe: a climatology, and ²²²Rn-based emission estimates, *Tellus*, 48, 457–473, 1996.
- Servant, J.: Temporal and Spatial Variations of the Concentration of the Short-Lived Decay Products of Radon in the Lower Atmosphere, *Tellus*, 18, 663–670, 1966.
- Sobyanina, E. V., Kovalenko, V. V., Maltsev, U. M., and Chechetkin, V. A.: Radon at the perspective development territory of the Severni microrraion in Minusinsk. Proceedings of the International Scientific Conference “Radioecology of the XXI century” – Krasnoyarsk, 14–16 May, 2012, SFU, 165–175, 2012.
- Somashekarappa, H. M., Narayana, Y., Radhakrishna, A. P., Siddappa, K., Joshi, V. B., Kholekar, R. V., and Bhagwat, A. M.: Atmospheric radon levels and its emanation rate in the environment of Kaiga, *Radiat. Meas.*, 26, 35–41, 1996.
- Szegvary, T., Leuenberger, M. C., and Conen, F.: Predicting terrestrial ²²²Rn flux using gamma dose rate as a proxy, *Atmos. Chem. Phys.*, 7, 2789–2795, doi:10.5194/acp-7-2789-2007, 2007.
- Tarasov, I. V.: Cement concretes and mortars with low natural radioactivity and radon permeability, M.S. thesis, Sib. Federal. Univ., Krasnoyarsk, 21, 2008.
- Taguchi, S., Law, R. M., Rödenbeck, C., Patra, P. K., Maksyutov, S., Zahorowski, W., Sartorius, H., and Levin, I.: TransCom continuous experiment: comparison of ²²²Rn transport at hourly time scales at three stations in Germany, *Atmos. Chem. Phys.*, 11, 10071–10084, doi:10.5194/acp-11-10071-2011, 2011.
- Turekian, K. K., Nozaki, Y., and Benninger, L. K.: The flux of radon and thoron from Australian Geochemistry of atmospheric radon and radon products, *Ann. Rev. Earth Planet Sci.*, 5, 227–255, 1977.
- Voevodin, V. A. and Kurguz, S. A.: Radon flux density variation from the soil in the measurement site of Krasnoyarsk. Proceedings of the International Scientific Conference “Radioecology of the XXI century” – Krasnoyarsk, 14–16 May, 2012, SFU, 108–114, 2012.
- Wilkniss, P. E., Larson, R. E., Bressan, P. J., and Steranka, J.: Atmospheric radon and continental dust near the automatic and their correlation with air mass trajectories, *J. Appl. Meteorol.*, 13, 512–520, 1974.
- Yakovleva, V. C.: The radon flux density from the Earth's surface as an indicator of a seismic activity, Proceedings of 7th International Conference on Gas Geochemistry – Freiberg, Germany, 22–26 September, 28–30, 2003.
- Yver, C., Schmidt, M., Bousquet, P., Zahorowski, W., and Ramonet, M.: Estimation of the molecular hydrogen soil uptake and traffic emissions at a suburban site near Paris through hydrogen, carbon monoxide, and radon-222 semicontinuous measurements, *J. Geophys. Res.*, 114, D18304, doi:10.1029/2009JD012122, 2009.